Available online at www.sciencedirect.com
SCIENCE DIRECT®
Physica D 194 (2004) 151–165
PHYSICA D
www.elsevier.com/locate/physd

A theoretical and experimental study on the unidirectional motion of a camphor disk

Masaharu Nagayama [a,*], Satoshi Nakata [b], Yukie Doi [b], Yuko Hayashima [b]

[a] *Research Institute for Mathematical Sciences, Kyoto University, Kitashirakawa, Sakyo-Ku, Kyoto 606-8502, Japan*
[b] *Department of Chemistry, Nara University of Education, Takabatake-cho, Nara 630-8528, Japan*

Received 7 July 2003; received in revised form 3 February 2004; accepted 4 February 2004
Communicated by Y. Kuramoto

Abstract

The self-sustaining motion of a camphor disk in an annular water channel was investigated. Unidirectional motion along the water channel is maintained after a local perturbation is applied to the system. Introduction of a partition into the channel changes the unidirectional motion into back-and-forth motion. To clarify the nature of the driving force that moves the settling camphor disk, the dependence of the velocity of the disk on the viscosity of the aqueous phase was measured. The experimental results are discussed in relation to the distribution of the camphor layer around the disk as the driving force. The nature of the self-motion is qualitatively reproduced by numerical computations using a mathematical model that incorporates the distribution of the camphor layer around the disk and the viscosity of the aqueous phase. Furthermore, the existence and stability of the unidirectional motion of the camphor disk depending on the viscosity of the aqueous phase are analyzed numerically.

MSC: 93A30; 70K50

Keywords: Self-motion; Reaction–diffusion model; Bifurcation; Traveling pulse

1. Introduction

The self-sustaining motion of liquid droplets [1–12], solid grains [13–21], and gels [22,23] has been investigated by simple experiments in attempts to both understand non-equilibrium systems and to invent novel chemomechanical transducers for isothermal conditions [24–26]. The spontaneous motion of a droplet or solid grain at an immiscible interface is generated by Marangoni flow [27–29], which is induced by non-uniformity of the concentration or a thermal gradient acting on the droplet or grain [1–21]. The details of this motion depend on the properties of the grain, such as its shape and chemical structure [14] and on external conditions, such as the shape and size of the cell, chemical stimuli, and temperature of the system [17–21]. Changes in these conditions can enhance the anisotropic distribution of the surface-active substance that is released from the droplet or solid grain. In this study, we examined the unidirectional motion around an annular water channel when a local perturbation is applied to a camphor disk. If

* Corresponding author. Tel.: +81-75-7537241; fax: +81-75-7537272.
E-mail address: nagayama@kurims.kyoto-u.ac.jp (M. Nagayama).

0167-2789/$ – see front matter © 2004 Elsevier B.V. All rights reserved.
doi:10.1016/j.physd.2004.02.003

a partition is placed in the water channel, the unidirectional motion becomes oscillatory. The velocity of the camphor disk was measured for various aqueous phase viscosities to investigate the effects of perturbation on camphor motion. These phenomena were numerically computed in relation to the spatial distribution of the camphor layer that forms on the air/water interface and the effect of viscosity as a driving force for motion. In addition, the existence and stability of the unidirectional camphor disk motion are demonstrated using a mathematical model. The relationship between camphor disk movement and viscosity is explained.

2. Experimental section

(+)-Camphor was obtained from Wako Chemicals (Kyoto, Japan). Water was first distilled and then purified using a Millipore Milli-Q filtering system (pH of the purified water: 6.3). A camphor disk (diameter 3 mm and thickness 1 mm) was prepared using a pellet die set and compression molding, and then carefully floated on the surface of water in an annular channel made of Teflon (channel width 5 mm, thickness 2 mm, inner radius 15 mm). The motion of the camphor disk was monitored using a digital video camera (SONY DCR-VX700) and recorded on videotape at 298 ± 1K. The two-dimensional position of the camphor was measured using a digitizer with a minimum time resolution of 1/30 s, and then analyzed by an image-processing system (Himawari, Library Inc., Japan).

3. Experimental results

Fig. 1(a) shows superimposed photographs of the motion of a camphor disk on the water phase. When the camphor disk was put on the water surface, the camphor disk did not move along the channel, but rather moved

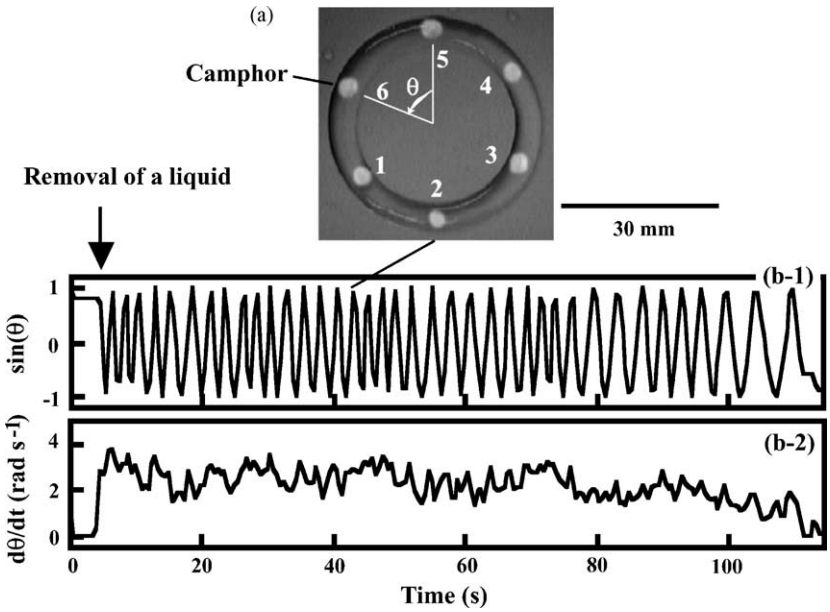

Fig. 1. (a) Superimposed photographs of camphor motion along a channel surface taken at a time interval of 1/3 s (numbered 1–6) (top view). (b) Time variation of the angular position of a camphor disk represented by (b-1) sin (θ) and (b-2) dθ/dt. In the initial stage, the camphor disk was at rest at $\theta = 0.57\pi$ (rad) ($\theta = 0$ is defined in (a)). Liquid (0.1 ml) was then removed from the water surface with a pipette at around $\theta = 0.7\pi$ at $t = 4$ s (indicated by an arrow). After removal, the camphor disk began moving around the channel in an anti-clockwise direction. Anti-clockwise motion was defined to have a positive velocity.

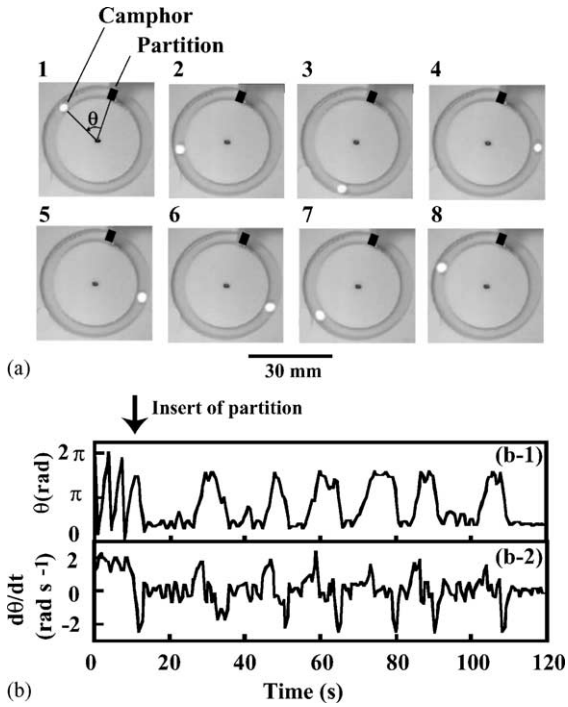

Fig. 2. (a) Photographs of camphor oscillation on a partitioned water channel taken at a time interval of 2 s (numbered 1–8) (top view). (b) Time variation of the angular position of the camphor disk represented by (b-1) θ and (b-2) $d\theta/dt$. In the initial stage, the camphor disk moved anti-clockwise around the water channel without a partition. When then the partition was inserted into the water channel at $t = 10$ s (indicated by an arrow), the motion of the camphor disk became oscillatory. The position of the partition was defined as $\theta = 0$ and anti-clockwise motion was defined to have a positive velocity.

in an oscillating manner between the inner and outer walls of the channel. Unidirectional movement began when some liquid (0.1 ml) was removed from the surface of the water next to the disk using a pipette (Fig. 1(b)). The camphor disk then moved toward the removal site, and maintained unidirectional motion at a uniform velocity (about 2 rad s^{-1}) for at least several tens of cycles, or about 1 min. After 80 s, the velocity of the disk began to decrease with time, and the camphor disk finally remained at one position in the channel.

Fig. 2 shows photographs of camphor oscillating around the water channel after the channel was divided by a partition. Initially, the partition was not used and unidirectional motion of the camphor disk was observed. After 10 s, a partition was inserted into the channel and the motion of the camphor became oscillatory, without the camphor colliding into the partition. Oscillatory motion (period: about 15 s) was maintained for 5–8 cycles, although the average velocity of motion decreased when the partition was inserted.

Fig. 3 shows the average velocity of the camphor disk as a function of the logarithm of relative viscosity (η_r). In this experiment, the average velocity was measured after the removal of a liquid as the perturbation (see Fig. 1). Channel properties were changed by adding various concentrations of glycerin to the water. To clarify the influence of surface tension, experiments were repeated with sodium dodecyl sulfate instead of glycerin to give a surface tension in the same range of 64.7–72.7 mN m^{-1} (data not shown). The strong decrease in average velocity appeared to be a result of an increase in viscosity rather than a decrease in surface tension.

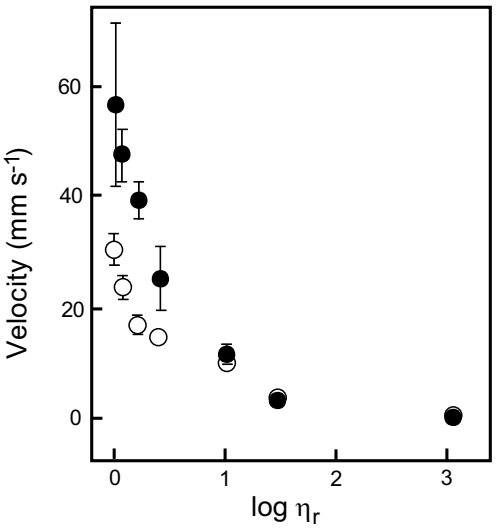

Fig. 3. Velocity of the self-sustained motion of camphor disks of diameter 3 mm (empty circles) and 13 mm (filled circles) as a function of relative viscosity ($\log \eta_r$). Aqueous phases of different viscosities were prepared using different concentrations of glycerin: 0, 1, 5, 8, 10, and 13.7 mol l^{-1}.

4. Discussion

The unidirectional motion of a camphor disk in a channel can be explained by the following mechanism [13,14]. (I) A camphor layer forms isotropically on the water surface around the disk, reducing the surface tension of the water. At this stage, the camphor disk is unable to move because the gradient of surface tension around the disk is isotropic and does not provide a driving force. (II) When some of the camphor layer is removed from one side of the disk, the camphor layer becomes anisotropic, and the isotropic surface tension gradient around the disk is broken. (III) The camphor disk then moves toward the region with a lower concentration of camphor at the surface (or higher surface tension) to reduce the spatial gradient of surface tension. (IV) When unidirectional motion starts, the camphor layer distribution remains anisotropic depending on the velocity. In addition, sublimation of the camphor layer from the water surface reduces the surface concentration of the camphor layer, which helps to produce uniform motion even after a large number of revolutions.

When the partition is introduced into the water channel, the camphor disk becomes sensitive to the partition as a boundary, and begins to move in an oscillatory fashion along the channel. Thus, the surface concentration of camphor layer near the partition increases as the camphor disk comes close to the boundary. Eventually, the concentration gradient across the disk reverses and the direction of motion changes.

It is necessary to disrupt the isotropy of the development of the camphor layer around the symmetric camphor disk in the symmetric cell to initiate motion of the stationary camphor disk, where the direction of motion is determined by the direction of the greatest perturbation in the camphor surface layer. Fig. 3 suggests that a water phase with a high viscosity reduces the velocity of this continuous motion. The high viscosity makes it more difficult to initiate motion of the camphor disk even when the external physical perturbation was applied to the camphor disk in this experiment. In fact, motion of a camphor disk in the high-viscosity water channel was difficult in general.

5. Computer-aided analysis of camphor disk motion

5.1. A mathematical model of the motion of a camphor disk

Based on a previous paper [20], we introduce a mathematical model for the self-sustaining motion of a camphor disk, as follows:

$$\rho S\ddot{\boldsymbol{x}}_{\mathrm{c}}(t) = S\nabla\gamma(u(\boldsymbol{x}_{\mathrm{c}}(t), t)) - \mu_{\mathrm{s}}\dot{\boldsymbol{x}}_{\mathrm{c}}(t), \tag{1}$$

where $\boldsymbol{x}_{\mathrm{c}}(t)$ is the center of the camphor disk, u the surface concentration of the camphor layer, ρ the surface density of the camphor disk (kg/m^2), S the area of top view of the disk (m^2), and μ_{s} the constant surface viscosity (kg/s) [30]. Surface tension at the air–water interface, γ, may be expressed as a simple function of $u(\boldsymbol{x}, t)$, as follows:

$$\gamma(u(\boldsymbol{x}_{\mathrm{c}}, t)) = \frac{\gamma_0}{a_0 u(\boldsymbol{x}_{\mathrm{c}}, t) + 1}, \tag{2}$$

where γ_0 is the surface tension of pure water and a_0 a positive constant.

The surface concentration of the camphor layer, which is produced by diffusion from the disk, decreases mainly by the sublimation of camphor molecules into the air, and to a lesser extent by dissolution into the water. Therefore, a model equation for the concentration of the camphor layer $u(\boldsymbol{x}, t)$ can be deduced from the reaction–diffusion equation, as follows [18,20]:

$$\frac{\partial u}{\partial t} = D\Delta u - k_0 u + F(\boldsymbol{x}_{\mathrm{c}}(t); r_0), \quad \boldsymbol{x} \in \Omega, t > 0, \tag{3}$$

where D is the diffusion coefficient of the camphor layer at the air/water interface, k_0 the sum of the rates of sublimation (k_1) and dissolution (k_2) of the camphor layer at the air/water interface ($k_0 = k_1 + k_2$), r_0 is the radius of the camphor disk, and Ω denotes the surface of the water channel. The function F, which is related to the flux of camphor from the camphor disk to the air/water interface, can be expressed by (4):

$$F(\boldsymbol{x}_{\mathrm{c}}(t); r_0) = \begin{cases} bS_0 & |\boldsymbol{x}_{\mathrm{c}}(t) - \boldsymbol{x}| \le r_0, \\ 0 & |\boldsymbol{x}_{\mathrm{c}}(t) - \boldsymbol{x}| > r_0, \end{cases} \tag{4}$$

where S_0 is the constant concentration of camphor at the disk surface and b the rate at which camphor is released from the disk into the camphor layer. The decrease in mass of the camphor disk by formation of the camphor layer is assumed to be negligible (i.e. where the mass of the disk is taken to be constant).

To normalize (1)–(4), we introduce the following dimensionless variables:

$$\tau = bt, \qquad \boldsymbol{y} = \sqrt{\frac{b}{D}}\boldsymbol{x}, \qquad v(\boldsymbol{y}, \tau) = \frac{u(\boldsymbol{x}, t)}{S_0}, \qquad \boldsymbol{y}_{\mathrm{c}}(\tau) = \sqrt{\frac{b}{D}}\boldsymbol{x}_{\mathrm{c}}(t), \tag{5}$$

where $\tau, \boldsymbol{y}, \boldsymbol{y}_{\mathrm{c}}, v$ and $\sqrt{b/D}\Omega = \{\sqrt{b/D}\boldsymbol{x}; \boldsymbol{x} \in \Omega\}$ have been rewritten as $t, \boldsymbol{x}, \boldsymbol{x}_{\mathrm{c}}, u$ and Ω, respectively. We then derive the following dimensionless system from (1)–(4):

$$\ddot{\boldsymbol{x}}_{\mathrm{c}}(t) = \nabla\gamma(u(\boldsymbol{x}_{\mathrm{c}}(t), t)) - \mu\dot{\boldsymbol{x}}_{\mathrm{c}}(t), \quad t > 0, \qquad \frac{\partial u}{\partial t} = \Delta u - ku + F(\boldsymbol{x}_{\mathrm{c}}(t); r), \quad \boldsymbol{x} \in \Omega, t > 0, \tag{6}$$

where F and γ are given by

$$F(\boldsymbol{x}_{\mathrm{c}}(t); r) = \begin{cases} 1 & |\boldsymbol{x}_{\mathrm{c}}(t) - \boldsymbol{x}| \le r, \\ 0 & |\boldsymbol{x}_{\mathrm{c}}(t) - \boldsymbol{x}| > r, \end{cases} \qquad \gamma(u(\boldsymbol{x}_{\mathrm{c}}, t)) = \frac{\gamma_1}{au(\boldsymbol{x}_{\mathrm{c}}, t) + 1} \tag{7}$$

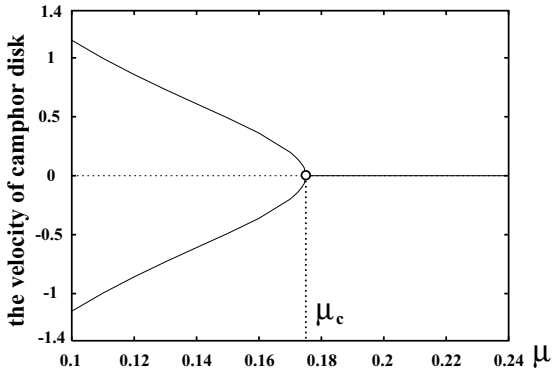

Fig. 4. Bifurcation diagram of camphor disk motion as a function of the parameter μ for $k = 0.1$, $r = 0.2$, $\gamma_1 = 2.0$, $a = 0.5$ and $R = 5.0$.

using the dimensionless parameters

$$k = \frac{k_0}{b}, \qquad \gamma_1 = \frac{\gamma_0}{\rho b D}, \qquad a = a_0 S_0, \qquad \mu = \frac{\mu_s}{\rho S b}, \qquad r = \sqrt{\frac{b}{D}} r_0. \tag{8}$$

To reproduce unidirectional motion along the annular channel, we consider the following one-dimensional initial and boundary value problems for (6) and (7):

$$\ddot{x}_c(t) = \frac{\partial}{\partial x}\left(\frac{\gamma_1}{a u(x_c, t) + 1}\right) - \mu \dot{x}_c(t), \quad t > 0, \qquad \frac{\partial u}{\partial t} = \frac{\partial^2 u}{\partial x^2} - k u + F(x_c(t); r), \quad 0 < x < 2\pi R, \quad t > 0 \tag{9}$$

and

$$F(x_c(t); r) = \begin{cases} 1 & |x_c(t) - x| \le r, \\ 0 & |x_c(t) - x| > r, \end{cases} \tag{10}$$

where the initial conditions

$$u(x, 0) \equiv 0, \quad 0 \le x < 2\pi R, \qquad (x_c(0), \dot{x}_c(0)) = (x_0, v_0), \tag{11}$$

periodic boundary conditions

$$u(0, t) = u(2\pi R, t), \qquad u_x(0, t) = u_x(2\pi R, t) \tag{12}$$

and regularity condition

$$u(\cdot, t) \in C^1([0, 2\pi R)) \tag{13}$$

are assumed. We take μ as a free parameter and choose suitable fixed values for r, γ_1, a, and R. Fig. 4 shows the bifurcation diagram of (9)–(13) obtained by numerical computation. For large values of μ, the camphor disk does not move. In this case, the spatial profile of the surface concentration of the camphor layer u is found to be symmetric with respect to $x_c(t)$, as shown in Fig. 5(a). For values of μ lower than μ_c, uniform unidirectional camphor disk motion replaces the absence of motion, and the velocity of the camphor disk gradually increases with decreasing μ. The direction of camphor motion is then determined by the sign of v_0, which corresponds to the perturbation

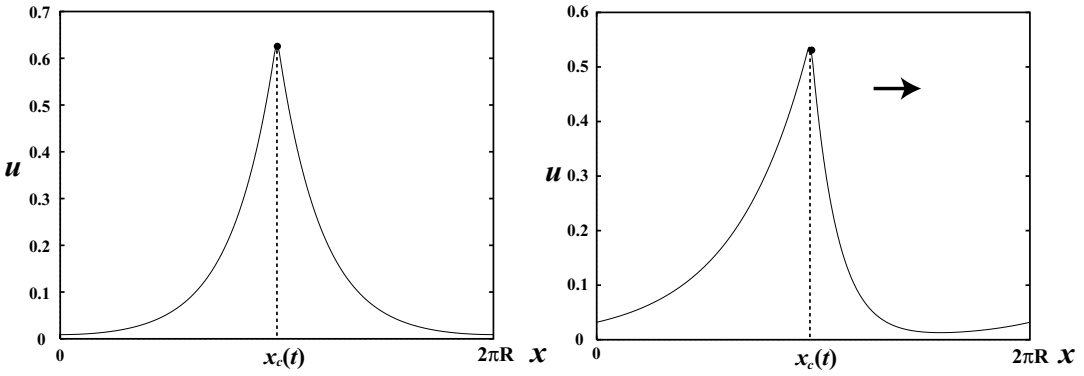

Fig. 5. Spatial profile of the surface concentration of camphor u around the camphor disk $x_c(t)$ for the same parameters as in Fig. 4 for (a) a motionless camphor disk ($\mu = 0.2$) and (b) uniform motion of a camphor disk ($\mu = 0.16$).

applied to the system in the experiments. Moreover, the spatial profile of u is no longer symmetric, as shown in Fig. 5(b).

We next consider the case in which a partition is inserted into the water channel. To describe this situation in our model, the boundary condition (12) is replaced by

$$\frac{\partial}{\partial x}u(0,t) = \frac{\partial}{\partial x}u(2\pi R,t) = 0, \quad t > 0. \tag{14}$$

Numerical simulation reveals that when the velocity of the camphor disk is slow, that is, μ is slightly less than μ_c, the camphor disk oscillates without colliding with the boundary, as shown in Fig. 6. However, when the velocity of the camphor disk is fast, that is, $0 < \mu \ll \mu_c$, the camphor disk collides with the boundary. In actual experiments, the camphor disk collides with the boundary when the viscosity is very low, which low viscosity conditions are realized by increasing the water temperature. Based on these results, we can conclude that our system of equations provides an appropriate model.

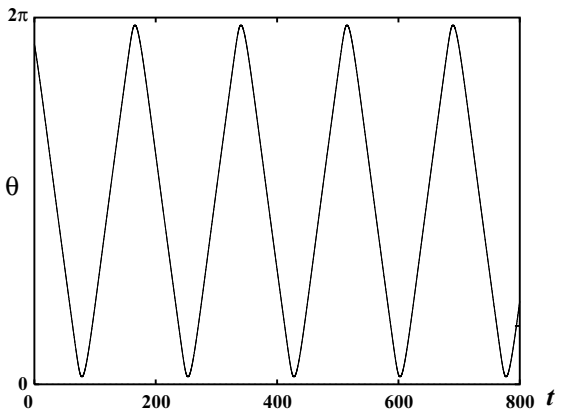

Fig. 6. Numerical results of oscillatory motion from (9)–(11) and (13) for the boundary condition (14) using the same parameters as in Fig. 5(b).

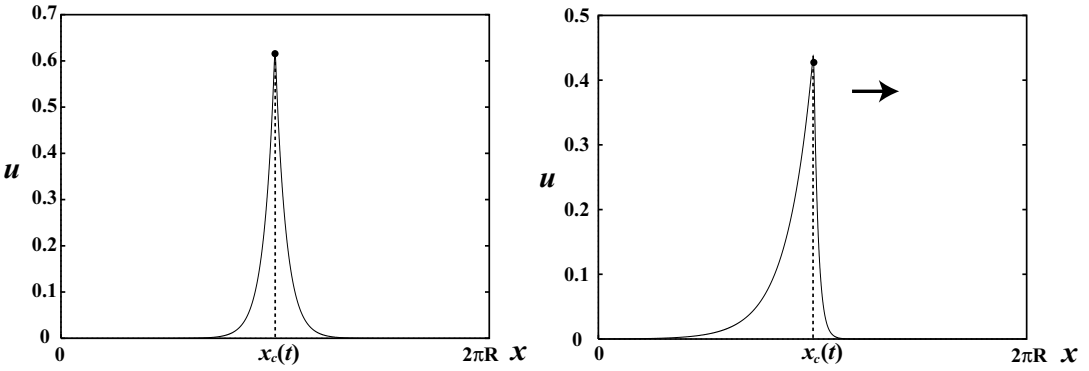

Fig. 7. Spatial profile of the surface concentration of camphor u around the position of the camphor disk $x_c(t)$ where the parameters are the same as those in Fig. 4 except that $R = 20.0$ for (a) a motionless camphor disk ($\mu = 0.2$) and (b) a camphor disk with uniform motion ($\mu = 0.16$).

5.2. Traveling pulse solution

To mathematically analyze the numerical results of camphor motion, we consider the following one-dimensional problem over the entire interval $\boldsymbol{R}$:

$$\ddot{x}_c(t) = \frac{\partial}{\partial x}\left(\frac{\gamma_1}{au(x_c,t)+1}\right) - \mu\dot{x}_c(t), \quad t > 0, \qquad \frac{\partial u}{\partial t} = \frac{\partial^2 u}{\partial x^2} - ku + F(x_c(t);r), \quad x \in \boldsymbol{R}, \ \ t > 0, \tag{15}$$

$$F(x_c(t);r) = \begin{cases} 1 & |x_c(t) - x| \le r, \\ 0 & |x_c(t) - x| > r \end{cases} \tag{16}$$

assuming the boundary condition

$$\lim_{|x|\to\infty} u(x,t) = 0 \tag{17}$$

and the regularity condition

$$u(\cdot,t) \in C^1(\boldsymbol{R}). \tag{18}$$

Under the boundary condition (12), if the central radius of an annular water channel R is sufficiently large, the spatial profile of u is well localized, as shown in Fig. 7. Moreover, when R is greater than 10, the velocity of the camphor disk is independent of R, as shown in Fig. 8. Therefore, we may safely replace the boundary condition (12) by (17).

A solution $[u(x,t), x_c(t)]$ of (15)–(18) is called a traveling pulse solution, if the form can be expressed as $u(x,t) = U(x-ct)$ and $x_c(t) = x_0 + ct$ where c is the velocity of the traveling pulse solution and x_0 is an arbitrary constant. This solution corresponds to uniform motion of the camphor disk. In particular, a traveling pulse solution is called a standing pulse when $c = 0$.

We take $z = x - ct$ and $z_c(t) = x_c(t) - ct$, and can set $z_c(t) = 0$ without loss of generality. Accordingly, traveling pulse solutions $(u(x,t), x_c(t)) = (U(z), x_0 + ct)$ with velocity c are obtained by solving the following equations derived from (15)–(18):

$$0 = \frac{-\gamma_1 a U_z(0)}{(aU(0)+1)^2} - \mu c, \tag{19}$$

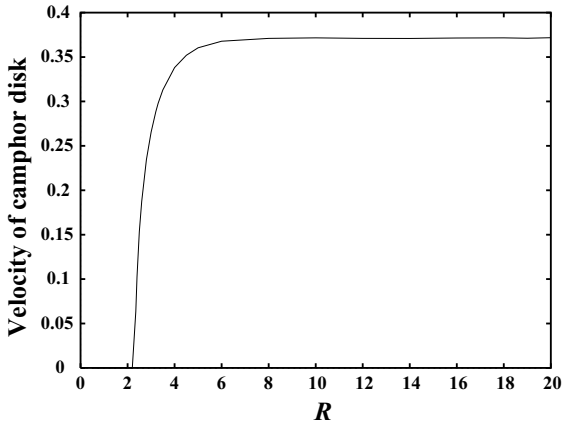

Fig. 8. The velocity of a camphor disk as a function of the radius of the circular water channel R, where the parameters are the same as those in Fig. 4 except for R.

$$-cU_z = U_{zz} - kU + F(0; r), \quad z \in \boldsymbol{R}, \tag{20}$$

$$F(0; r) = \begin{cases} 1 & |z| \le r, \\ 0 & |z| > r, \end{cases} \tag{21}$$

$$\lim_{|z|\to\infty} U(z) = 0, \tag{22}$$

$$U(\cdot) \in C^1(\boldsymbol{R}). \tag{23}$$

For a fixed parameter c, we obtain the unknown U from (20)–(23):

$$U(z) = \begin{cases} A_1 \exp(\frac{1}{2}\nu_+ z) & -\infty < z < -r \\ A_2 \exp(\frac{1}{2}\nu_+ z) + B_2 \exp(\frac{1}{2}\nu_- z) + \dfrac{1}{k} & -r \le z \le r, \\ B_3 \exp(\frac{1}{2}\nu_- z) & r < z < \infty, \end{cases} \tag{24}$$

where

$$A_1 = \frac{\nu_-}{2k\nu}\left(\exp\left(-\frac{\nu_+}{2}r\right) - \exp\left(\frac{\nu_+}{2}r\right)\right), \qquad A_2 = \frac{\nu_-}{2k\nu}\exp\left(-\frac{\nu_+}{2}r\right),$$
$$B_2 = -\frac{\nu_+}{2k\nu}\exp\left(\frac{\nu_-}{2}r\right), \qquad B_3 = \frac{\nu_+}{2k\nu}\left(\exp\left(-\frac{\nu_-}{2}r\right) - \exp\left(\frac{\nu_-}{2}r\right)\right) \tag{25}$$

and $\nu = \nu(c) = \sqrt{c^2 + 4k}$ and $\nu_\pm = \nu_\pm(c) = (-c \pm \nu(c))$. Substituting (24) into (19), we get the following equation for c:

$$0 = \frac{-\gamma_1 a U_z(0)}{(aU(0) + 1)^2} - \mu c \equiv G(c; \mu), \tag{26}$$

where

$$U(0) = \frac{1}{k}\left(\frac{\nu_-}{2\nu}\exp\left(-\frac{\nu_+}{2}r\right) - \frac{\nu_+}{2\nu}\exp\left(\frac{\nu_-}{2}r\right) + 1\right) \tag{27}$$

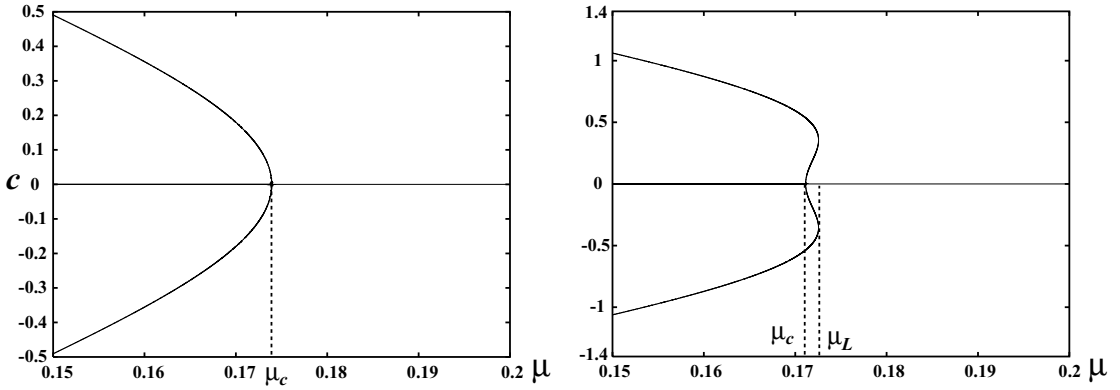

Fig. 9. Global solution structure of the equation $G(c;\mu) = 0$ for the same parameters as in Fig. 4 except for r. (a) Supercritical pitch-fork bifurcation for $r = 0.2$. (b) Subcritical pitch-fork bifurcation for $r = 1.6$.

and

$$U_z(0) = \frac{1}{\nu}\left(\exp\left(\frac{\nu_-}{2}r\right) - \exp\left(-\frac{\nu_+}{2}r\right)\right). \tag{28}$$

It is obvious that $c = 0$ is a solution of (26) for any $\mu > 0$. This yields a standing pulse solution for (20)–(23), which corresponds to the stationary state of the camphor disk. We now take μ and r as free parameters and keep k, γ_1 and a constant. When r is small, we find numerically that a critical value μ_c exists such that the traveling pulse solution in (19)–(23) exists for $\mu < \mu_c$. The traveling pulse solution bifurcates supercritically from the standing pulse solution at $\mu = \mu_c$, as shown in Fig. 9(a). However, when r is large, the bifurcation diagram changes from supercritical to subcritical, as shown in Fig. 9(b). This result suggests that two traveling pulse solutions exist simultaneously for $\mu_c < \mu < \mu_L$, and the two solutions differ by the magnitude of the velocity. To investigate if the type of bifurcation changes from supercritical to subcritical, we expand $G(c;\mu) = 0$ with small c, and obtain the following relationship up to $O(c^3)$:

$$c(\mu - \mu_c) + g(r;k)c^3 + O(c^5) = 0, \tag{29}$$

where

$$\mu_c = \gamma_1 a \frac{r\exp(-\sqrt{k}r)}{2\sqrt{k}(a\beta(r,k)+1)^2} > 0 \tag{30}$$

and

$$g(r;k) = \frac{\gamma_1 a}{6}\frac{r\exp(-\sqrt{k}r)}{(a\beta(r,k)+1)^2}\left(\frac{1}{4}\left(\frac{3r}{2\sqrt{k}} - r^2\right) + \frac{3}{a\beta(r,k)+1}\left(\frac{k+a}{4k^2} - \left(\frac{ar^2}{2k} + \frac{ar}{2k\sqrt{k}} + \frac{a}{4k^2}\right)\mathrm{e}^{-\sqrt{k}r}\right)\right) \tag{31}$$

with $\beta(r,k) = (1 - \exp(-\sqrt{k}r))/k (> 0)$.

We now fix $k > 0$, and easily obtain

$$g(0;k) = 0$$

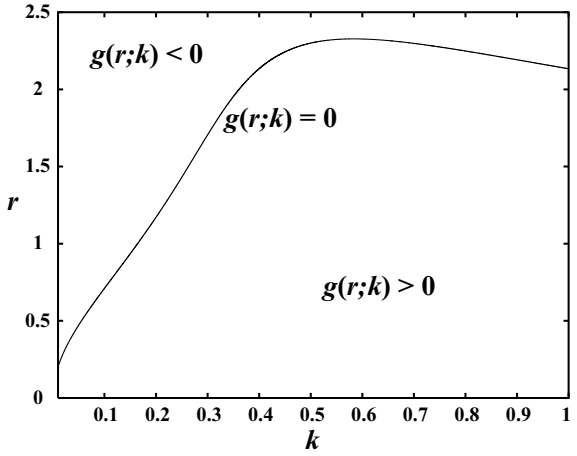

Fig. 10. Nullcline of $g(r; k) = 0$ where $\gamma_1 = 2.0$, $a = 0.5$.

and

$$\frac{\partial g}{\partial r}(0; k) = \frac{\gamma_1 a}{6}\left(\frac{3}{4k}\right) > 0.$$

Moreover,

$$g(r; k) < \frac{\gamma_1 a r\, \mathrm{e}^{-\sqrt{k}r}}{6}\left(\frac{1}{4}\left(\frac{3r}{2\sqrt{k}} - r^2\right) + 3\frac{k+a}{4k^2}\right) \tag{32}$$

$$g(r; k) < 0 \quad \text{for } r > \frac{1}{4}\left(\frac{3}{\sqrt{k}} + \frac{\sqrt{57k + 48a}}{k}\right) \equiv r_2. \tag{33}$$

Hence, we find that there exist r_1 and r_2 such that $g(r; k) > 0$ for $0 < r < r_1$ and $g(r; k) < 0$ for $r > r_2$. Therefore, we obtain the following proposition:

Proposition 1. *For arbitrary fixed γ_1, a and $k > 0$, the following conditions hold*: (i) *if $0 < r < r_1$, $G(c; \mu) = 0$ has a supercritical pitch-fork bifurcation at μ_c; and* (ii) *if $r > r_2$, $G(c; \mu) = 0$ has a subcritical pitch-fork bifurcation at μ_c.*

The nullcline of $g(r; k) = 0$ is plotted in Fig. 10. From this and Proposition 1, the traveling pulse is shown to bifurcate supercritically from the standing pulse when r is small, and to bifurcate subcritically when r is large.

5.3. Stability of the traveling pulse solution

In this section, we consider the stability of the traveling pulse solution. Let $\{U(z), 0, c\}$ be a traveling pulse solution of (15)–(18), where $z = x - ct$ is the moving coordinate. We formally derive a linearized problem of (15)–(18) around $\{U(z), 0, c\}$ to obtain the following eigenvalue problem:

Find $\lambda \in \boldsymbol{C}$, $\phi \in \boldsymbol{C}$, $\psi \in \boldsymbol{C}$ and $\alpha \in H^1(\boldsymbol{R})$ such that

$$\lambda\alpha = \alpha_{zz} + c\alpha_z - k\alpha, \tag{34}$$

$$\lambda\phi = \psi, \tag{35}$$

$$\lambda\psi = -\frac{\gamma_1 a}{(aU(0)+1)^3}(A\phi + B) - \mu\psi \tag{36}$$

with jump condition

$$\alpha_z(r+0) - \alpha_z(r-0) = -\phi(r), \qquad \alpha_z(-r+0) - \alpha_z(-r-0) = -\phi(-r), \tag{37}$$

where we set

$$A = U_{zz}(0)(a\beta(r,k)+1) - 2aU_z^2(0) \tag{38}$$

and

$$B = \alpha_z(0)(a\beta(r,k)+1) - 2aU_z(0)\alpha(0). \tag{39}$$

Solving (34) with respect to α and substituting the result into (35) and (36), we obtain

$$\lambda\phi = \psi, \qquad \lambda\psi = -\frac{\gamma_1 a}{(a\beta(r,k)+1)^3}(A + C(\lambda))\phi - \mu\psi, \tag{40}$$

where we set

$$C(\lambda) = \omega(\lambda)(a\beta(r,k)+1) - 2aU_z(0)\delta(\lambda) \tag{41}$$

and

$$\omega(\lambda) = \frac{1}{\kappa_+ - \kappa_-}\left(\kappa_+ \exp(-\kappa_+ r) - \kappa_- \exp(\kappa_- r)\right), \tag{42}$$

$$\delta(\lambda) = \frac{1}{\kappa_+ - \kappa_-}(\exp(-\kappa_+ r) - \exp(\kappa_- r)) \tag{43}$$

and $\kappa_\pm = \kappa_\pm(\lambda; c)$ are two solutions of the characteristic equation, $x^2 + cx - (k+\lambda) = 0$ ($\mathrm{Re}\,\kappa_- < 0 \le \mathrm{Re}\,\kappa_+$).

We therefore obtain the following nonlinear equation for the eigenvalues of (34)–(36):

$$\lambda(\lambda+\mu) + \frac{\gamma_1 a}{(a\beta(r,k)+1)^3}(A + C(\lambda)) = 0. \tag{44}$$

We easily find that $\lambda = 0$ is a solution of (44) for any parameters μ, which correspond to the translational freedom of traveling pulse solutions. We numerically searched for solutions of (44) other than $\lambda = 0$. As a result, the following stability of traveling and standing pulse solutions was found:

Case I Fig. 11(a) shows the stability of solutions of (15)–(18) when r is small. The standing pulse solution $\{U(z), 0, 0\}$ is stable when $\mu > \mu_c$ is fixed; i.e., (44) has no positive eigenvalues except for the trivial eigenvalue 0. When $\mu < \mu_c$ is fixed, (44) has one positive real eigenvalue and the standing pulse solution is unstable. However, the traveling pulse solution $\{U(z), 0, c(\neq 0)\}$ is stable for $0 < \mu < \mu_c$.

Case II Fig. 11(b) shows the stability of the solutions of (15)–(18) when r is large. The stability of the standing pulse solution is the same as in Case I. When $\mu_c < \mu < \mu_L$, two traveling pulse solutions with different velocities exist. The traveling pulse solution for the larger velocity is stable, while the slow traveling pulse solution is unstable, with the fast solution stable for all $0 < \mu \le \mu_c$.

With parameters corresponding to Case I, a motionless camphor disk begins to move slowly in one direction as the viscosity decreases. In this case, a single traveling pulse moves periodically without colliding with the boundary in a sufficiently large finite interval, as shown in Fig. 6. The existence of such a periodic solution is shown using the

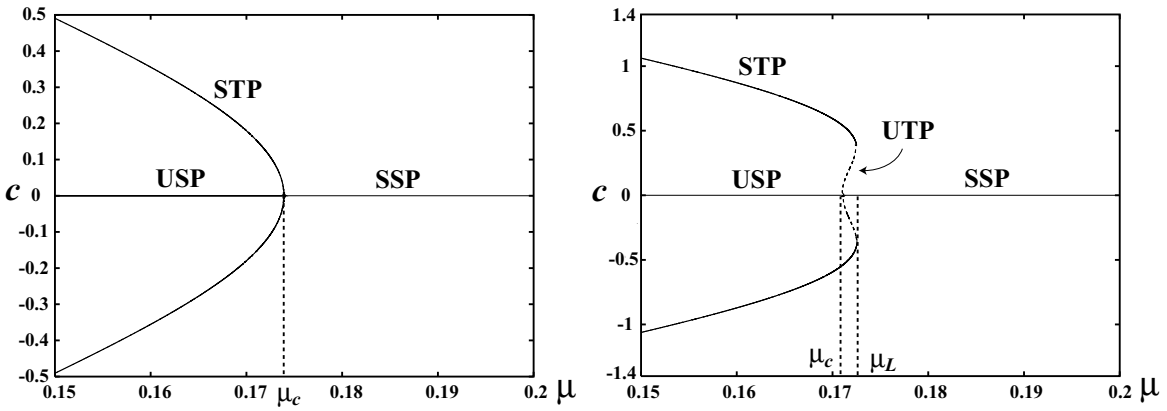

Fig. 11. Global structure and stability of solutions of (15)–(18) for the same parameters as in Fig. 4, except that (a) $r = 0.2$ and (b) $r = 1.6$. SSP: stable standing pulse solution, USP: unstable standing pulse solution, STP: stable traveling pulse solution, UTP: unstable traveling pulse solution.

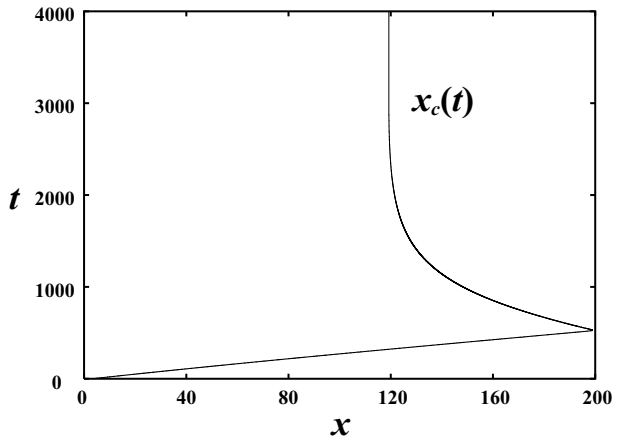

Fig. 12. Transition of the motion of $x_c(t)$ with the non-flux boundary condition for $k = 0.02$, $r = 0.5$, $\gamma_1 = 2.0$, $a = 0.5$ and $\mu = 0.235$.

pulse interaction approach [31]. In some parameter region in Case II, we found a traveling pulse solution which, however, becomes a standing pulse solution after the reflection at the boundary, as shown in Fig. 12. We have not yet obtained the analytical explanation of such a motion of pulse.

6. Conclusion

A camphor disk maintains unidirectional motion upon the application of an initial perturbation without a partition, and oscillatory motion with a partition, while spontaneously disrupting the isotropic distribution of the camphor layer along the water channel. To clarify the mechanisms behind these phenomena, a theoretical simulation based on a coupled system using the reaction–diffusion equation and Newton's equations of motion was carried out, as a function of the surface concentration of the camphor layer calculated in this system. We succeeded in qualitatively

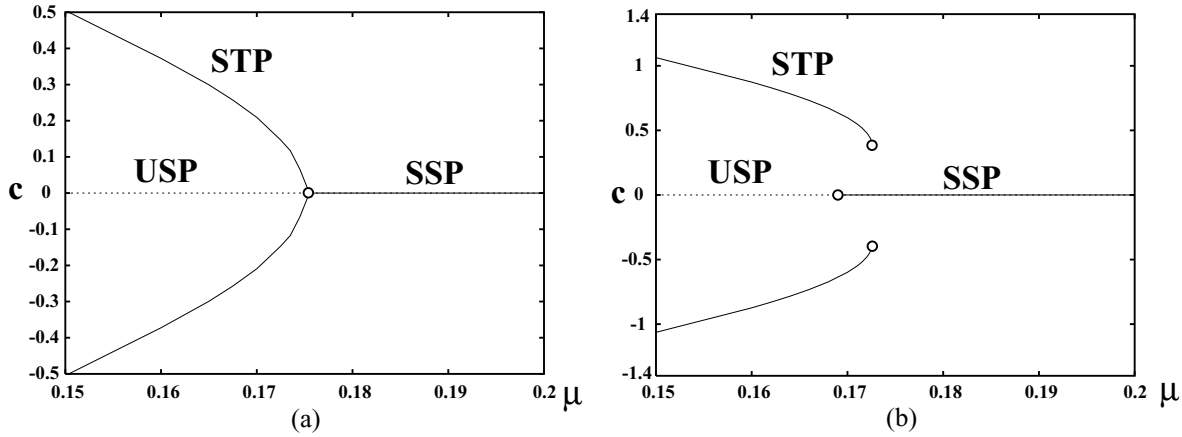

Fig. 13. Bifurcation diagram of (9)–(13) as a function of the parameter μ for $k = 0.1, \gamma_1 = 2.0, a = 0.5$, and $R = 20.0$. (a) Supercritical bifurcation from a stable standing pulse to a stable traveling pulse at $r = 0.2$. (b) Subcritical bifurcation at $r = 1.6$.

reproducing the spontaneous motion of a camphor disk by a numerical simulation. Furthermore, by computer-aided analysis, we proved the existence and stability of traveling pulse solutions corresponding to the unidirectional motion of a camphor disk in the experiments. Although the stability analysis was mathematically incomplete, the numerical simulation of (9), (10) and (13) is thought to justify the results of the stability analysis, as shown in Fig. 13. Finally, we studied the bifurcation phenomena of a camphor disk as a function of the viscosity of the water phase. The mathematical results suggest that bifurcations occur super- and subcritically with respect to the viscosity, for small and large camphor disks, respectively, as shown in Fig. 11. However, the experimental results suggest that bifurcations in the present system depend on viscosity, as shown in Fig. 3. We could not determine if these bifurcations were super- or subcritical based on the experimental results, since it is extremely difficult to construct a completely circular camphor disk and to reduce thermal fluctuation. In addition, the existence of currents and convection in the water, which are neglected in the model, make this task even more difficult.

Acknowledgements

We thank Mr. H. Kitahata (Kyoto University, Japan) for his technical assistance, Prof. M. Mimura (Hiroshima University, Japan), Prof. H. Okamoto (Kyoto University, Japan) and Prof. Y. Yamada (Kyoto University, Japan) for providing useful suggestions, and Prof. T. Ikeda (Ryukoku University, Japan) for providing technical feedback on the stability analysis. M. Nagayama is supported in part by a Grant-in-Aid for Scientific Research from the Ministry of Education, Science and Culture of Japan #14740070. S. Nakata is supported in part by a Grant-in-Aid for Scientific Research from the Ministry of Education, Science and Culture of Japan #14540559.

References

[1] M. Dupeyrat, E. Nakache, Direct conversion of chemical energy into mechanical energy at an oil water interface, Bioelectroch. Bioenerg. 5 (1987) 134–141.
[2] S. Kai, E. Ooishi, M. Imasaki, Experimental study of nonlinear waves on interface between two liquid phases with chemical reaction, J. Phys. Soc. Jpn. 54 (1985) 1274–1281.
[3] T. Yamaguchi, T. Shinbo, A novel interfacial engine between two immiscible liquids, Chem. Lett. (1989) 935–938.
[4] N. Magome, K. Yoshikawa, Nonlinear oscillation and ameba-like motion in an oil/water system, J. Phys. Chem. 100 (1996) 19102–19105.

[5] S. Nakata, H. Komoto, K. Hayashi, M. Menzinger, Mercury drop “attacks” an oxidant crystal, J. Phys. Chem. B 104 (2000) 3589–3593.
[6] Yu.Yu. Stoilov, Fluorocarbons as volatile surfactants, Langmuir 14 (1998) 5685–5690.
[7] Yu.Yu. Stoilov, Oscillation of evaporating liquids and ispalator paradoxes, Phys. Uspekhi 43 (2000) 39–53.
[8] K.D. Barton, R.S. Subramanian, The migration of liquid drops in a vertical temperature gradient, J. Colloid. Interf. Sci. 133 (1989) 211–222.
[9] M.K. Chaudhury, G.M. Whitsides, How to make water run uphill, Science 256 (1992) 1539–1541.
[10] F.D.D. Santos, T. Ondarcuhu, Free-running droplets, Phys. Rev. Lett. 75 (1995) 2972–2975.
[11] P.-G. Gennes, Wetting: Statics and dynamics, Rev. Mod. Phys. 57 (1985) 827–863.
[12] V.G. Levich, in: D.B. Spalding (Ed.), Physicochemical Hydrodynamics, Advance Publications Limited, London, 1977.
[13] L.J.W.S. Rayleigh, Measurements of the amount of oil necessary in order to check the motions of camphor upon water, Proc. R. Soc. London 47 (1890) 364–367.
[14] S. Nakata, Y. Iguchi, S. Ose, M. Kuboyama, T. Ishii, K. Yoshikawa, Self-rotation of a camphor scraping on water: new insight into the old problem, Langmuir 13 (1997) 4454–4458.
[15] S. Nakata, Y. Hayashima, Spontaneous dancing of a camphor scraping, J. Chem. Soc., Faraday Trans. 94 (1998) 3655–3658.
[16] S. Nakata, Y. Iguchi, S. Ose, T. Ishii, pH-sensitive self-motion of a solid scraping on an aqueous phase, J. Phys. Chem. B 102 (1998) 7425–7427.
[17] S. Nakata, Y. Hayashima, Spontaneous motion of a solid is sensitive to the pH of an aqueous phase, Langmuir 15 (1999) 1872–1875.
[18] S. Nakata, Y. Hayashima, H. Komoto, Spontaneous switching of camphor motion between two chambers, Phys. Chem. Chem. Phys. 2 (2000) 2395–2399.
[19] S. Nakata, M.I. Kohira, Y. Hayashima, Mode selection of a camphor boat in a dual-circle canal, Chem. Phys. Lett. 322 (2001) 419–423.
[20] Y. Hayashima, M. Nagayama, S. Nakata, A camphor grain oscillates while breaking symmetry, J. Phys. Chem. B 105 (2001) 5353–5357.
[21] M.I. Kohira, Y. Hayashima, M. Nagayama, S. Nakata, Synchronized self-motion of two camphor boats, Langmuir 17 (2001) 7124–7129.
[22] R. Yoshida, T. Takahashi, T. Yamaguchi, H. Ichijo, Self-oscillating gel, J. Am. Chem. Soc. 118 (1996) 5134–5135.
[23] R. Yoshida, M. Tanaka, S. Onodera, T. Yamaguchi, E. Kokufuta, In-phase synchronization of chemical and mechanical oscillations in self-oscillating gels, J. Phys. Chem. A 104 (2000) 7549–7555.
[24] K. Sekimoto, Langevin equation and thermodynamics, Prog. Theor. Phys. 130 (1998) 17–27.
[25] K. Yoshikawa, H. Noguchi, A working hypothesis on the mechanism of molecular machinery, Chem. Phys. Lett. 303 (1999) 10–14.
[26] R.D. Astumian, M. Bier, Fluctuation driven ratchets: molecular motors, Phys. Rev. Lett. 72 (1994) 1766–1769.
[27] E. Sackmann, in: L. Rensing, N.I. Jaeger (Eds.), Temporal Order, Springer-Verlag, Berlin, 1985, p. 153.
[28] L.E. Scriven, C.V. Sternling, The marangoni effects, Nature 187 (1960) 186–188.
[29] L.D. Landau, E.M. Lifshits, Fluid Mechanics, 2nd ed., Course of Theoretical Physics, vol. 6, Pergamon Press, London, 1987.
[30] C. Barentin, C. Ybert, J. Meglio, J. Joanny, Surface shear viscosity of Gibbs and Langmuir monolayers, J. Fluid. Mech. 397 (1999) 331–349.
[31] S.-I. Ei, M. Mimura, M. Nagayama, Pulse–pulse interaction in reaction–diffusion systems, Physica D 165 (2002) 176–198.